Available online at www.sciencedirect.com
ScienceDirect
Ceramics International 36 (2010) 961–968
CERAMICS INTERNATIONAL
www.elsevier.com/locate/ceramint

Structure and thermal properties of heat treated plasma sprayed ceria–yttria co-stabilized zirconia coatings

Giovanni Di Girolamo *, Caterina Blasi, Monica Schioppa, Leander Tapfer

ENEA, Department of Advanced Physics, Technologies and New Materials, Brindisi Research Centre, S.S. 7 Appia, km 713.7, 72100 Brindisi, Italy

Received 24 September 2009; received in revised form 8 October 2009; accepted 24 October 2009
Available online 20 November 2009

Abstract

Thick plasma sprayed thermal barrier coatings are suitable for thermal and hot corrosion protection of metal components in land-based turbine and diesel engines. In this work, ceria–yttria co-stabilized zirconia coatings were deposited by atmospheric plasma spraying in a mixture of non-transformable tetragonal t′ and cubic c zirconia phases. Free-standing coatings were isothermally annealed at 1315 °C for different times and their crystal structure was studied by XRD. No phase decomposition occurred. Columnar grains grew in the molten splats with increasing annealing time according to a preferential direction and, after 50 h of heat treatment, they were partially replaced by equiaxed grains. Both in-plane and out-of-plane thermal expansion coefficients (CTEs) were measured from coating expansion during heating. The CTE was slightly sensitive to thermal exposure in out-of-plane direction, whereas it kept almost constant in plane direction. The specific heat capacity *Cp* of annealed coatings, measured by differential scanning calorimetry (DSC), decreased in comparison with as-sprayed coating, due to high-temperature sintering.

Keywords: C. Thermal properties; D. ZrO_2; E. Thermal applications; Plasma spraying

1. Introduction

Thermal barrier coatings (TBCs) are currently used to extend the lifetime of Ni-based superalloys components operating in severe environments in land-based turbine and diesel engines. In addition, they represent potential solutions to increase the engine efficiency, in terms of higher combustion temperature and reduced cooling air flow, and to reduce the fuel consumption. Further new applications concern glass-melting furnaces' components, such as heat exchangers and valves, which have to be protected against high temperature and hot gases.

Severe operating conditions can reduce the performance of state-of-the-art yttria partially stabilized zirconia (YSZ) coatings. These last ones are typically constituted by non-transformable tetragonal t′ zirconia phase in as-sprayed condition. During exposure at temperature of about 1300 °C, t′ phase transforms to a high-yttria cubic phase and a low-yttria tetragonal phase. On slow cooling to room temperature, the low-yttria tetragonal phase may transform to the monoclinic phase, whereas the high-yttria cubic phase may be retained or it may transform to a high-yttria tetragonal t′ phase [1]. The volume change, associated to the monoclinic transition, promotes cracking, leading the TBC system to spallation and, finally, to catastrophic failure. In addition, high-temperature sintering of the porous microstructure may reduce its strain tolerance. These shortcomings of YSZ involve the search for alternative TBC materials. Several compositions are currently studied, however, up to now no composition which realizes a better compromise than YSZ in all the relevant thermo-mechanical properties demanded to TBC materials has been found [2–9]. Indeed, all these materials are better than zirconia only in one or two properties.

To this purpose, some rare earth oxides with fluorite structure, and mainly CeO_2, can be added to zirconia to stabilize its tetragonal and cubic phase, thus providing high-temperature phase stability. Among the various compositions investigated in the last years, ceria and yttria co-stabilized zirconia (CYSZ) is particularly promising when severe operating conditions are expected. It has been found that CYSZ coatings show higher phase stability and thermal shock resistance than YSZ ones, because the phase transition is

* Corresponding author. Tel.: +39 0831 201503; fax: +39 0831 201581.
E-mail address: giovanni.digirolamo@enea.it (G. Di Girolamo).

0272-8842/$36.00
doi:10.1016/j.ceramint.2009.10.020

retarded and occurs at a little extent [10–14]. An enhanced hot corrosion resistance has been also noticed [15].

Thicker TBCs are particularly promising for land-based turbine components, which experience long exposure at high temperature. The increase in coating thickness represents an easy solution in order to tolerate larger thermal gradients and to reduce the requirements for air cooling system. A reduction of about 60% has been quantified for 1.5 mm thick TBCs [16]. The microstructure of a thick coating can be tailored for the desired performance by control of spraying parameters. Coatings with high porosity and uniform crack distribution are typically characterized by low thermal conductivity and Young's modulus, and, therefore, they possess an enhanced strain tolerance at high temperature [17,18]. Obviously, the failure of a thick coating is rather complex and different from that of a thin coating [19]. The mismatch between the thermal expansion coefficients (CTEs) of ceramic top coat and metal bond coat governs the failure mechanism of a thick coating rather than the growth and the evolution of a thermally grown oxide (TGO) at their interface [20]. The evolution of thermal stresses within the TBC influences its service life and, moreover, it is strongly related to high-temperature phase changes, grain growth and sintering of the porous microstructure. Thereby, all these aspects have to be carefully investigated by TBC designers.

In this paper, thick CYSZ coatings were deposited by atmospheric plasma spraying (APS) and isothermally heat treated at high temperature up to 50 h, since the effects of thermal aging on the microstructure are emphasized within the first 25–50 h of heat treatment and, then, they slow down as the coating is partially sintered [21,22]. The phase stability and the thermo-physical properties of CYSZ coatings, such as thermal expansion coefficient and specific heat capacity, were investigated and related to the annealing time, since the thermal transport properties are strongly related to the evolution of the microstructure. Quantitative Rietveld analysis was performed in order to study the evolution of the crystallite size and microstrains during high-temperature coating exposure.

2. Experimental procedure

2.1. Plasma spraying

Ceria–yttria co-stabilized zirconia coatings were deposited on stainless steel substrates (25 mm × 25 mm × 4 mm) by atmospheric plasma spray (Sulzer Metco, Wolhen, Switzerland) equipped with F4-MB plasma torch with a 6 mm internal diameter nozzle. The feedstock was the commercial ZrO_2–$25CeO_2$–$2.5Y_2O_3$ HOSP (Metco 205NS, Sulzer Metco, Westbury, NY) and the coating thickness was 2 mm. CYSZ particles are spherical and showed dimensions ranging from 10 μm to 110 μm. An intermediate bond coat was previously deposited with a thickness of 160 μm (38Co–32Ni–21Cr–8Al–0.5Y, Amdry 995C, Sulzer Metco, Westbury, NY). Before spraying, the substrates were grit-blasted with abrasive alumina powder (Metcolite F, Sulzer Metco, Westbury, NY) and ultrasonically cleaned in ethanol. Then, they were placed on a rotating sample holder and coated. The plasma spray parameters are summarized in Table 1. The optimal plasma spray parameters for CYSZ feedstock have been set by using an empirical method, based on previous experiments. In particular, the carrier gas flow rate and the rotation speed of powder feeder stirrer and disk have been set with the purpose to achieve a powder feed rate of about 45 g/min and to deposit an average thickness of 13 μm per torch pass. An air cooling jet (pressure = 5 bar) was used in order to reduce the coating temperature during deposition. Before heat treatment, the coatings were cut to the desired dimensions and stripped off from their substrates by chemical etching, by using a 50/50 HCl–H_2O solution. The acid attacked the interface between bond coat and top coat. Then, the detached ceramic coatings were cleaned by rinsing and infiltration of water, acetone and ethanol, in sequence, to remove acid residue and other contaminants. Free-standing coatings were then isothermally annealed at 1315 °C in an air furnace for 2, 10, 20 and 50 h, at heating rate of 6 °C/min and then slowly furnace cooled down to room temperature.

Table 1
Plasma spray parameters used in this work.

Parameter	CoNiCrAlY	CYSZ
Current (A)	600	600
Voltage (V)	71.4	70
Turntable velocity (rad/s)	50	100
Substrate tangential speed (mm/s)	1041	2083
Gun velocity (mm/s)	4	4
Primary gas Ar flow rate (slpm)	55	38
Secondary gas H_2 flow rate (slpm)	11	11
Stand off distance (mm)	120	120
Carrier gas flow rate (slmp)	3	2.6
Powder feeder disk rotation (% of max)	18	23
Powder feeder stirrer rotation (% of max)	80	90
Powder feed rate (g/min)	49.7	44
Injector diameter (mm)	1.8	1.8
Injector angle (°)	90	90
Distance torch-injector (mm)	6	6

2.2. Structural and microstructural analyses

Phase composition of as-sprayed and annealed CYSZ coatings was investigated by using an X-ray powder diffractometer (PW1880, Philips, Almelo, Netherlands) operating with Cu Kα radiation produced at 40 kV and 40 mA. A first scan was performed between 20°and 80° with a step of 0.02°. Scans at higher resolutions were also performed, at 0.01° in the range from 27° and 32° and at 0.005° between 71° and 75°, respectively. Quantitative structural analysis was carried out by using the Rietveld technique and the free-domain Maud software [23]. The Rietveld refinement was performed following the guidelines of McCusker et al. [24]. Due to the overlapping between tetragonal t′ and cubic c zirconia phases, the Rietveld refinement can result very difficult and tedious and the best solution was to analyze the coating structure in well-determined 2θ ranges, where the different phases were well observable and quantifiable. The (2 0 0) and (4 0 0) reflections

were the most suitable peaks for quantitative analysis. To this purpose, the (4 0 0) crystalline peaks were deconvoluted and analyzed in the range 71–75°. The peak shape was fitted with a pseudo-Voigt function convoluted with an asymmetric function, whereas the background was adjusted by a five-parameter polynomial function. The instrumental parameters, including three Caglioti parameters for full-width at half-maximum (FWHM), two asymmetry factors and two parameters for Gaussian content of peak profiles, were fixed to the values obtained for standard material used to determine the instrumental broadening.

The lattice parameters, the crystallite size and the r.m.s. microstrains were refined for both tetragonal and cubic zirconia phases, as well the fractional z coordinate of the O^{2-} anion in the tetragonal asymmetric unit. The R_p parameter, representative of the goodness of fitting, was calculated after removing the background contribution. It should be noted that surface roughness may generate a microabsorption effect, *i.e.* a reduction of the peak intensity, especially at low angles. B-factors (isotropic temperature factor) were fixed for each element to standard values, without modifying the quality of the fit [25,26].

The fractured cross-section of as-sprayed and annealed CYSZ coatings was analyzed by means of scanning electron microscopy (XL40, Philips, Eindhoven, Netherlands), after cutting by a low speed diamond blade and metallization by the deposition of a very thin gold film. The polished cross-section of as-sprayed coating was cold-mounted in vacuum in polymer, ground using diamond discs and polished to 0.25 μm.

2.3. Thermo-physical properties

Various measurement techniques were employed for the determination of the thermo-physical properties of as-sprayed and annealed CYSZ coatings. For determination of the thermal expansion, the samples were analyzed with a Netzsch dilatometer (Model TMA 402, Netzsch-Gerätebau GmbH, Selb, Germany). The system here employed is mounted vertically and consists of a linear variable displacement transducer (LVDT) with thermo-stated housing. Changes in length of a sample caused by expansion or shrinkage move the quartz pushrod on the ferrite core of LVDT and cause an electrical signal in its coil. This electrical signal is amplified and recorded as a change in length. The temperature of the sample is measured and recorded by a thermocouple. Thermal expansion measurements were carried out in static air on free-standing samples 5–8 mm long and 2 mm thick, at a 5 °C/min rate up to 900 °C. Both in-plane and out-of-plane thermal expansion coefficients were measured. To check the accuracy of the pushrod dilatometer three measurements in the same conditions were carried out on a synthetic sapphire (NS SRM 732) from room temperature to 900 °C. The calculated mean linear expansion coefficient was compared with the mean value of the standard material reported in the literature ($9.2 \times 10^{-6}\,K^{-1}$). The accuracy was equal to 3%. For the determination of specific heat capacity and for DSC analysis of CYSZ samples, the Simultaneous Thermal Analyzer (Model STA 429, Netzsch-Gerätebau GmbH, Selb, Germany) equipped with a sample holder for differential scanning calorimetry (type *S* sensor) was used. Eq. (1) constitutes the ratio method and may be used to determine the specific heat of the material directly from the STA data [27]:

$$Cp_s = Cp_{\mathrm{std}}(m_{\mathrm{std}}/m_{\mathrm{s}})(\Delta T_s/\Delta T_{\mathrm{std}}) \quad (1)$$

The subscript std indicates the sapphire standard, s indicates the sample, ΔT are the ordinate deflections from the sample, standard and baseline, and m indicates the mass. DSC samples were approximately cut to 3 mm × 3 mm × 2 mm. The sample weight used for Cp and DSC curves was approximately 120 mg, and the measurements were done in static air using Pt crucibles with lids, at 20 °C/min heating rate. The measurements were performed from room temperature up to 1200 °C. As standard reference material a synthetic sapphire disc was used (Cp of sapphire at 20 °C: 0.775 J/g K—NBS literature value). Three consecutive measurements cycles were performed for each sample.

3. Results and discussion

3.1. Structural and microstructural analyses

The whole XRD spectra in the range between 20° and 80° of as-sprayed and annealed coatings are shown in Fig. 1. Fig. 2a shows the low-angle 27–32° range of XRD patterns, whereas Fig. 2b shows the high-angle 71–75° range. As-sprayed coatings are composed of a mixture of tetragonal t′ and cubic c zirconia phases, according to Joint Committee on Powder Diffraction Standards (JCPDS) Nos. 81-1544 and 49-1642 cards, available at International Centre for Diffraction Data (ICDD). A very small amount of cubic CeO_2 is also detected (JCPDS 81-0792), but not indicated in the pattern. The overlapping between tetragonal and cubic zirconia peaks may make rather difficult their deconvolution. The cubic to

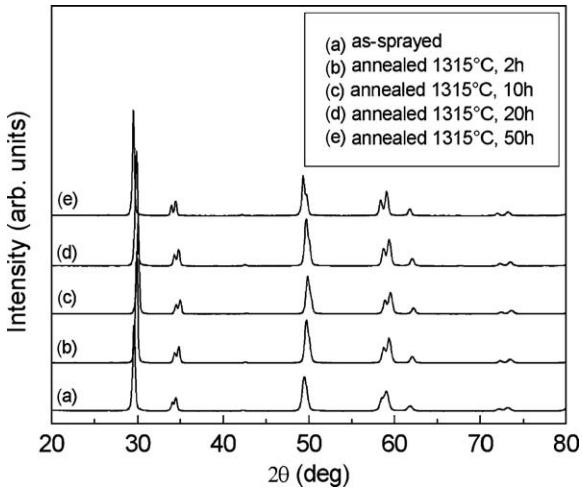

Fig. 1. XRD spectra in the range between 20° and 80° of as-sprayed and annealed CYSZ coatings.

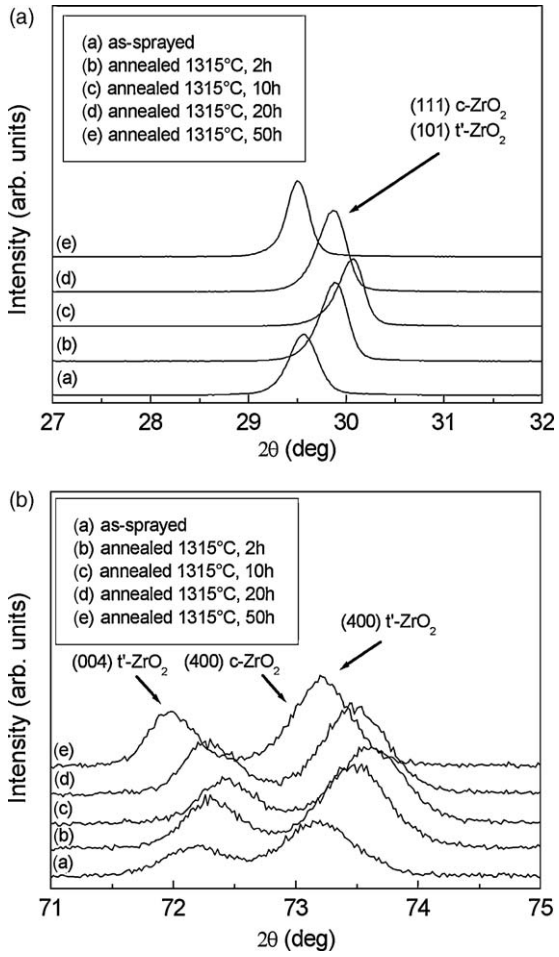

Fig. 2. (a) Low-angle region and (b) high-angle region of XRD patterns.

tetragonal ratio, calculated by deconvolution of (4 0 0) reflections, is around 16%. These results are in good agreement with results reported by others [28]. The difference in cubic fraction is explained in terms of different spraying parameters. The tetragonal t′ phase arose from high quenching rate of molten droplets upon impact on the substrate. During plasma spraying, part of high-temperature cubic phase was transferred to metastable tetragonal t′ phase by a fast diffusionless transformation, without any composition change. The remaining part of high-temperature cubic c zirconia phase was retained at room temperature. It should be noted that some chemical reactions take place during deposition of CYSZ coatings. High-temperature processes commonly promote changes in valence state, *i.e.* the reduction of Ce^{4+} ions to Ce^{3+} ions. However, during spraying a partial re-oxidation of Ce^{3+} ions to Ce^{4+} ions occurs at the coating surface and it results in the decrease of oxygen vacancies and cubic phase content. After plasma spraying, the light-gray colour of the feedstock changed in yellow which is the typical colour of a ZrO_2–CeO_2–Y_2O_3 solution. Ce^{3+} cation and the resulting oxygen vacancies play an important role in the stabilization of the cubic phase, whereas Ce^{4+} ions are able to stabilize zirconia in the tetragonal form, as described by Choi et al. in a previous work [12,29].

Table 2
Lattice parameters and volume fraction for tetragonal and cubic zirconia phases in as-sprayed and annealed coatings.

Parameter	As-sprayed	Annealed			
		2 h	10 h	20 h	50 h
$a_{T'}$	3.65	3.64	3.64	3.64	3.66
$c_{T'}$	5.24	5.23	5.22	5.23	5.25
a_C	5.19	5.17	5.17	5.17	5.19
Volume fraction T' (%)	84	86	86	91	92
Volume fraction C (%)	16	14	14	9	8
R_P	9.13	9.01	8.38	8.06	9.21

The addition of CeO_2 stabilizer to zirconia produces a distortion effect and an increase in lattice parameters for tetragonal and cubic phases. There is a shift of their peaks' position towards small angles in comparison with standard tetragonal and cubic zirconia phases. Indeed, the lattice parameters of CYSZ are located between the correspondent values of YSZ and pure CeO_2 (a = 5.4113 Å). Table 2 shows the lattice parameters and the relative volume fraction for both tetragonal t′ and cubic c zirconia phases, as obtained from Rietveld analysis.

XRD results show no phase decomposition after isothermal annealing. Indeed, looking at the 27–32° range, no monoclinic phase is detectable. The tetragonal to monoclinic transformation is promoted by crystallite growth and only occurs when the grain size becomes higher than a critical value [30]. Slight changes can be observed in the 71–75° range, as consequence of crystallite size growth and evolution of microstrains. Part of the cubic fraction is transferred to tetragonal t′ phase. This transformation is strongly related to the local microstructure of each coating. Indeed, the stabilizer content may fluctuate within the lamellae and this can explain any discrepancy in the results of quantitative analysis.

Fig. 3 illustrates the r.m.s microstrains versus annealing time for tetragonal and cubic phases. The fluctuation of the lattice parameters from grain to grain, associated to the presence of a distribution of stabilizer content inside crystallites, produces

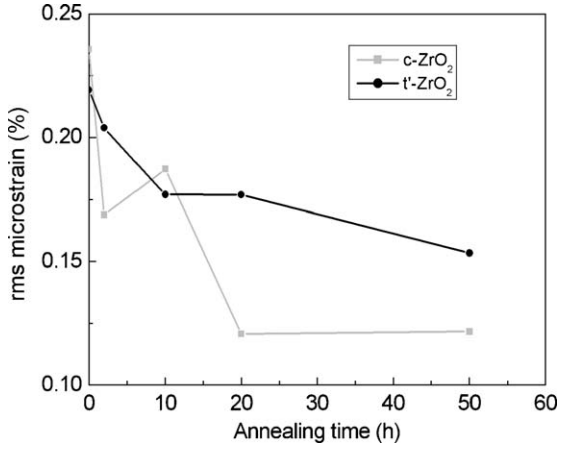

Fig. 3. Microstrains versus annealing time for tetragonal and cubic zirconia phases.

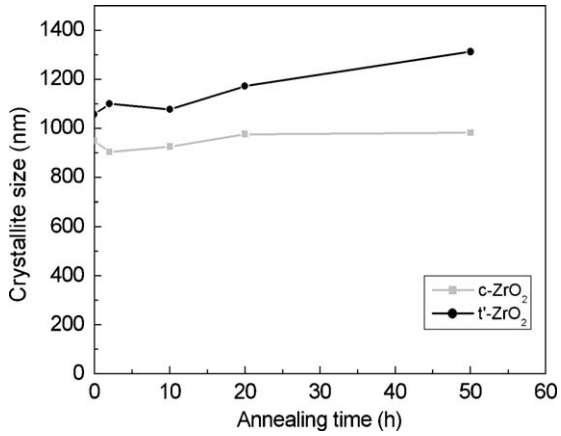

Fig. 4. Crystallite size versus annealing time for tetragonal and cubic zirconia phases.

the microstrains. These microstrains are larger in as-sprayed conditions, due to higher lattice distortion, and then they are partially released during thermal aging, due to lattice stress relaxation. In annealed YSZ coatings an increase in microstrain for t′ phase has been noticed, resulting from the diffusion of the yttria stabilizer, the reduction of the tetragonal t′ zirconia phase and the increase of other phases, such as cubic phase and low-yttria tetragonal phase. It has been also reported that the microstrain level in cubic YSZ phase decreases. For CYSZ coatings, the mechanism seems to be different, at least in the first 50 h of their thermal exposure, due to the reduction of the cubic phase. These values of microstrains are not high enough to allow crack formation and propagation.

Fig. 4 shows the relationship between crystallite size and annealing time for both zirconia phases. The grain size increases with annealing time due to the thermal aging, even if this increase is not particularly large. It should be noted that the crystallites are much smaller than columnar grains. Structural changes can be also related to sintering and crystal lattice scale.

Fig. 5 shows a SEM micrograph of the entire TBC, composed of metal substrate, bond coat and CYSZ top coat.

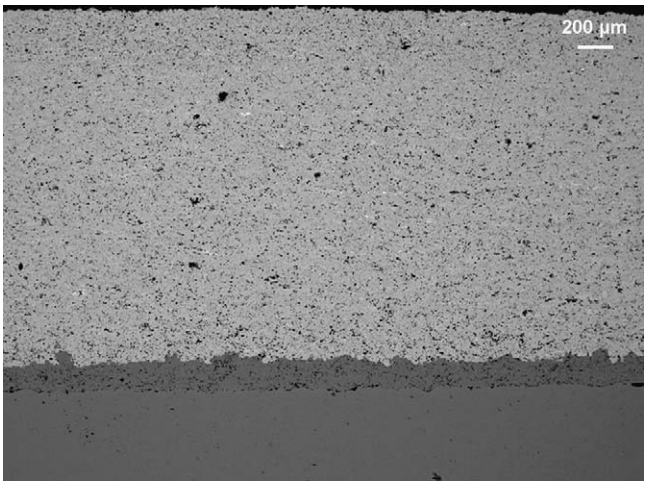

Fig. 5. Microstructure of thick CYSZ thermal barrier coating.

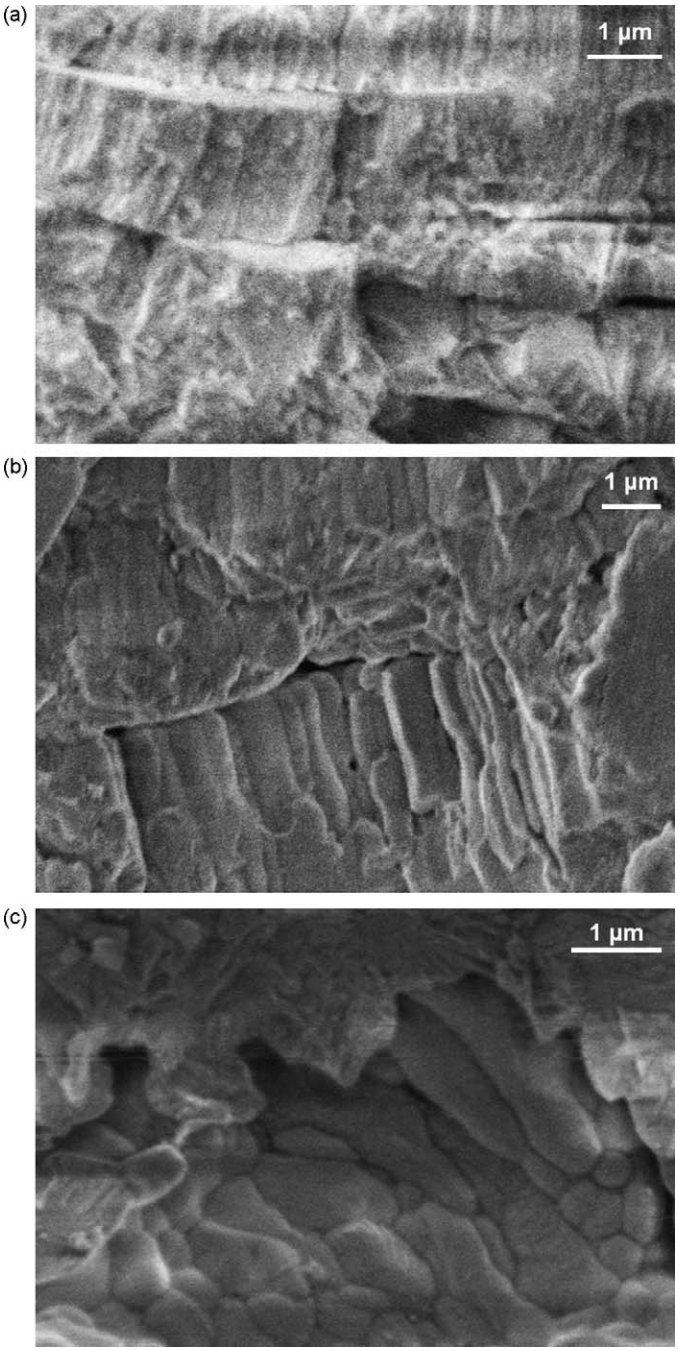

Fig. 6. Fractured cross-section of (a) as-sprayed, (b) 10 h annealed and (c) 50 h annealed CYSZ coatings.

SEM secondary electron images reported in Fig. 6 show the fractured cross-section for as-sprayed and annealed coatings. The as-sprayed CYSZ coating shows a lamellar structure composed of lamellae approximately parallel to coating–substrate interface, separated by splat boundaries and embedded in a network of cracks and voids. The thickness of the lamellae is approximately between 0.5 μm and 4.5 μm. Within molten splats columnar grains can be observed. They possess a preferential direction, since they are oriented from the bottom to the top of the splats. The length and the thickness of each lamella increase with increasing annealing time, by the gradual growth of these columnar grains across splat

boundaries. After 50 h, grain rotation among neighboring grains occurs, producing a coherent grain–grain interface, the disappearance of grain boundaries and, consequently, grain coalescence. A similar behaviour has been appreciated for plasma sprayed nanostructured YSZ coatings [31]. The grain orientation changes and some equiaxed grains grow and replace the columnar structure that tends to disappear. Moreover, a transgranular fracture is observed in the CYSZ coatings after high-temperature exposure.

3.2. Thermo-physical properties

The in-plane and through-thickness thermal expansions of as-sprayed, 10 and 50 h annealed CYSZ coatings are shown in Figs. 7 and 8, respectively. In-plane and out-of-plane thermal expansions are almost linear between 50 °C and 900 °C for both as-sprayed and annealed coatings. No in situ sintering occurs up 900 °C. It should be noted that the presence of small impurities in the starting feedstock and then in as-sprayed and heat treated coatings is not observable by XRD analysis, however, it can surely affect the thermal expansion of the samples during heating. The thermal expansion coefficients in 50–900 °C range are summarized in Table 3. The thermal expansion coefficient is sensitive to the thermal aging in the out-of-plane direction and varies from $10.1 \times 10^{-6}\,K^{-1}$ to $12.5 \times 10^{-6}\,K^{-1}$. Otherwise, the thermal expansion coefficient is rather constant in plane direction. It should be noted that the out-of-plane CTE is affected by interlamellar cracks which run between coating lamellae, whereas the in-plane CTE is affected by vertical cracks. High-temperature sintering produces the closure of interlamellar porosity and mainly affects out-of-plane shrinkage, without providing significant changes in plane direction. Moreover, the distribution of vertical microcracks and pores within the CYSZ coating is rather uniform and yields to similar high-temperature features along orthogonal directions.

The in-plane CTE of CYSZ coatings is larger than that of YSZ coatings reported in literature and calculated using the same procedure. This enhancement can be explained in terms of different structure, *i.e.* the presence of cubic structure and higher concentration of oxygen vacancies. Indeed, changes in crystal structure and valence state can influence the thermal expansion, also explaining the slight differences in CTE of as-sprayed and annealed CYSZ coatings. Guo et al. [18] have reported a value of $11.2 \times 10^{-6}\,K^{-1}$ in plane direction for as-sprayed and annealed YSZ coatings between room temperature and 1200 °C, since the thermal expansion coefficient was not affected by coating microstructure in their experiment. Their coatings were only heat treated at 1200 °C for 10 h. The same coatings showed high segmentation crack density, even if their porosity was comparable to our coatings. Moreover, the values measured in this work are higher than those of CYSZ coatings reported in literature [32]. As an example, Ahmaniemi et al. have measured a CTE of $10.8 \times 10^{-6}\,K^{-1}$ in plane direction between 50 °C and 1000 °C for other CYSZ coatings [33]. The results herein discussed are notably promising, since a larger CTE is surely able to reduce the stresses arising from the thermal expansion mismatch between top coat and bond

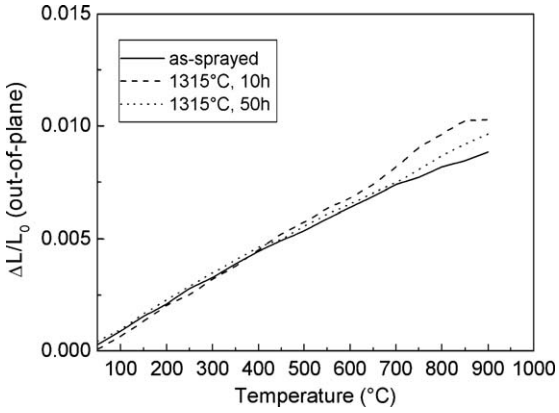

Fig. 8. Out-of-plane thermal expansion of as-sprayed and annealed CYSZ coatings.

Table 3
In-plane and out-of-plane thermal expansion coefficients for as-sprayed and annealed coatings.

Coating	α_X (50–900 °C) [$10^{-6}\,K^{-1}$]	α_Z (50–900 °C) [$10^{-6}\,K^{-1}$]
As-sprayed	12.62	10.13
1315 °C, 10 h	12.14	12.45
1315 °C, 50 h	12.64	10.69

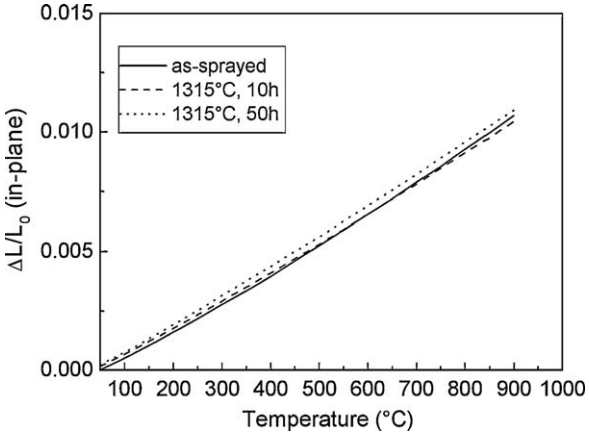

Fig. 7. In-plane thermal expansion of as-sprayed and annealed CYSZ coatings.

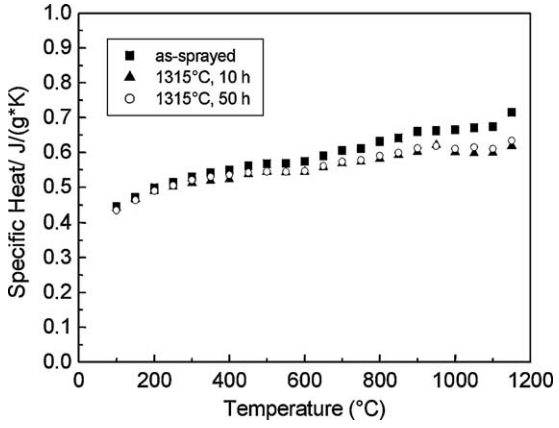

Fig. 9. Specific heat capacity of as-sprayed and annealed CYSZ coatings.

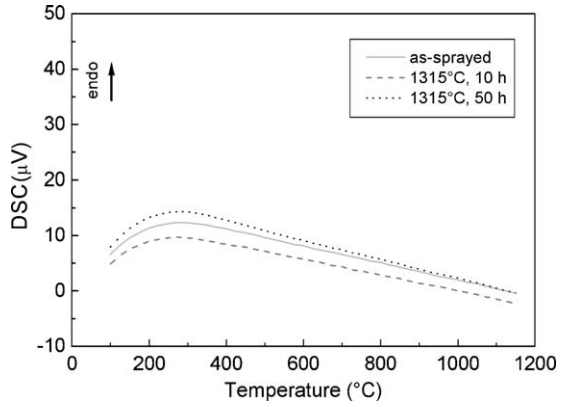

Fig. 10. DSC curves of as-sprayed and annealed CYSZ coatings.

coat, thus increasing the lifetime of TBC during thermal cycling.

The averages of specific heat capacity measurements on as-sprayed and thermally aged CYSZ coatings are illustrated in Fig. 9. *Cp*(*T*) curves were calculated as a mean value of three consecutive measurement cycles. It can be seen that the specific heat increases gradually as the temperature increases. At any given temperature, below 600 °C, there appears to be no distinct difference of specific heat between as-sprayed and thermally aged CYSZ coatings. The specific heat capacity curves above 600 °C clearly show a sensitive variation between as-sprayed and annealed coatings, which may be associated to grain growth, high-temperature sintering and densification of the porous microstructure, since all these effects affect the heat transmission mechanism through the anisotropic microstructure. Until now, it has been reported that *Cp* is not sensitive to the coating microstructure. For as-sprayed coatings, *Cp* is around $0.44\ J\ K^{-1}\ g^{-1}$ at 100 °C and $0.71\ J\ K^{-1}\ g^{-1}$ at 1150 °C. This values are almost similar to those found for other plasma sprayed YSZ coatings [34]. However, high-temperature specific heat capacity decreases for heat treated coatings. This variation is in the range between 11% and 13.5%. The aging time seems not to influence the heat capacity, suggesting very close microstructural and thermal properties for coatings aged up to 50 h. Thereby, high-temperature aging reduces the heat capacity of CYSZ coatings by sintering of the porous microstructure. The formation of sintering necks between the lamellae and/or the disappearance of splat boundaries result in a decrease of interlamellar porosity and a better contact between the same lamellae, thus influencing the thermal transport properties [35]. In conclusion, the CYSZ coatings show a relatively contained high-temperature sintering. No phase transformations are detectable in DSC curves, as shown in Fig. 10.

4. Conclusions

Ceria–yttria co-stabilized thick thermal barrier coatings were sprayed by atmospheric plasma spray and annealed at 1315 °C for different times. CeO_2 provided a high phase stabilization for zirconia, since no phase decomposition was observed after thermal aging. No monoclinic phase was formed and the cubic c phase of as-sprayed coatings was partially transferred to tetragonal t′. As annealing time increased, crystallite size increased, whereas a reduction in microstrains was appreciated. Columnar grains were observed in as-sprayed coatings. They grew with increasing annealing time according to a preferential direction and were partially replaced by equiaxed grains after 50 h of heat treatment.

The thermal expansion of as-sprayed and heat treated coatings was rather linear and the thermal expansion coefficient changed after thermal aging in out-of-plane direction, while it kept almost constant in plane direction. Indeed, its average was in the range from $12.1 \times 10^{-6}\ K^{-1}$ to $12.6 \times 10^{-6}\ K^{-1}$ in plane direction and from $10.1 \times 10^{-6}\ K^{-1}$ to $12.5 \times 10^{-6}\ K^{-1}$ through coating thickness. The thermal expansion coefficient of CYSZ coatings was higher than those reported for other YSZ and CYSZ coatings and, therefore, more close to that of the bond coat material. Lower strains are then expected during long-term high-temperature exposure of tri-layered TBC system and, correspondingly, an enhanced lifetime. Specific heat capacity *Cp* was sensitive to the microstructure and decreased for high-temperature annealed coatings, due to the first-stage sintering of the porous microstructure. The CYSZ coatings showed a relatively contained high-temperature sintering. The effect of high-temperature sintering on the microstructure and mechanical properties of CYSZ coatings will be discussed in a separate investigation.

Acknowledgements

The authors would like to thank Pierangela Caliandro (OPTEL) for her valuable technical assistance in SEM observations.

References

[1] U. Schulz, Phase transformation in EB-PVD yttria partially stabilized zirconia thermal barrier coatings during annealing, J. Am. Ceram. Soc. 83 (4) (2000) 904–910.
[2] X.Q. Cao, R. Vassen, D. Stoever, Ceramic materials for thermal barrier coatings, J. Eur. Ceram. Soc. 24 (2004) 1–10.
[3] D. Stover, G. Pracht, H. Lehmann, M. Dietrich, J.E. Doring, R. Vassen, New material concepts for the next generation of plasma-sprayed thermal barrier coatings, J. Thermal Spray Technol. 13 (1) (2004) 76–83.
[4] D.R. Clarke, C.G. Levi, Materials design for the next generation thermal barrier coatings, Annu. Rev. Mater. Res. 33 (2003) 383–417.
[5] C.G. Levi, Emerging materials and processes for thermal barrier systems, Curr. Opin. Solid State Mater. Sci. 8 (2004) 77–91.
[6] M.O. Jarligo, D.E. Mack, R. Vassen, D. Stover, Application of plasma-sprayed complex perovskites as thermal barrier coatings, J. Thermal Spray Technol. 18 (2) (2009) 187–193.
[7] R. Vassen, A. Stuke, D. Stover, Recent developments in the field of thermal barrier coatings, J. Thermal Spray Technol. 18 (2) (2009) 181–186.
[8] S. Paul, A. Cipitria, S.A. Tsipas, T.W. Clyne, Sintering characteristics of plasma sprayed zirconia coatings containing different stabilizers, Surf. Coat. Technol. 203 (2009) 1069–1074.
[9] R.S. Lima, B.R. Marple, Nanostructured YSZ thermal barrier coatings engineered to counteract sintering effects, Mater. Sci. Eng. A 485 (2008) 182–193.
[10] C.H. Lee, H.K. Kim, H.S. Choi, H.S. Ahn, Phase transformation and bond coat oxidation behavior of plasma-sprayed zirconia thermal barrier coatings, Surf. Coat. Technol. 124 (2000) 1–12.

[11] R. Taylor, J.R. Brandon, P. Morrell, Microstructure, composition and property relationship of plasma sprayed thermal barrier coatings, Surf, Coat. Technol. 50 (1992) 141–149.
[12] H. Choi, H. Kim, C. Lee, Phase evolutions of plasma sprayed ceria and yttria stabilized zirconia thermal barrier coating, J. Mater. Sci. Lett. 21 (2002) 1359–1361.
[13] J. Moon, H. Choi, H. Kim, C. Lee, The effects of heat treatment on the phase transformation behavior of plasma-sprayed stabilized ZrO_2 coatings, Surf. Coat. Technol. 155 (2002) 1–10.
[14] B. Ma, Y. Li, K. Su, Characterization of ceria–yttria stabilized zirconia plasma-sprayed coatings, Appl. Surf. Sci. 255 (2009) 7234–7237.
[15] S. Sodeoka, M. Suzuki, T. Inoue, K. Ueno, S. Oki, Thermal and mechanical properties of plasma sprayed ZrO_2–CeO_2–Y_2O_3 coatings, in: C.C. Berndt (Ed.), Proceedings of the 9th National Thermal Spray Conference: Thermal-Spray, Practical Solutions for Engineering Problems, Cincinnati USA, October 96, ASM International, Materials Park, OH, 1996, pp. 295–302.
[16] P. Bengtsson, J. Wigren, Segmentation cracks in plasma sprayed thick thermal barrier coatings, in: P.J. Maziasz, I.G. Wright, et al. (Eds.), Proceedings of ASM Materials Solutions: Gas Turbine Materials Technology, Rosemont, Italy, (1999), p. 92.
[17] D. Schwingel, R. Taylor, T. Haubold, J. Wigren, C. Gualco, Mechanical and thermophysical properties of thick PYSZ thermal barrier coatings: correlation with microstructure and spraying parameters, Surf. Coat. Technol. 108/109 (1998) 99–106.
[18] H.B. Guo, R. Vassen, D. Stover, Thermophysical properties and thermal cycling behavior of plasma sprayed thick thermal barrier coatings, Surf. Coat. Technol. 192 (2005) 48–56.
[19] T.M. Yonushonis, Thick thermal barrier coatings for diesel components, NASA CR-187111, August 1991.
[20] A. Rabiei, A.G. Evans, Failure mechanism sssociated with the thermally grown oxide in plasma-sprayed thermal barrier coatings, Acta Mater. 48 (2000) 3963–3976.
[21] R.W. Trice, Y.J. Su, R. Mawdsley, K.T. Faber, A.R. De Arellano-Lopez, H. Wang, W.D. Porter, Effect of heat treatment on phase stability, microstructure and thermal conductivity of plasma-sprayed YSZ, J. Mater. Sci. 37 (11) (2002) 2359–2365.
[22] H. Wang, R.B. Dinwiddie, Characterization of thermal barrier coatings using thermal methods, Adv. Eng. Mater. 3 (7) (2001) 465–468.
[23] Material Analysis Using Diffraction, version 2.074, Luca Lutterotti, University of Trento, Italy (2009).
[24] L.B. McCusker, R.B. Von Dreele, D.E. Cox, D. Louer, P. Scardi, Rietveld refinement guidelines, J. Appl. Cryst. 32 (1999) 36–50.
[25] D.G. Lamas, G.E. Lascalea, R.E. Juarez, E. Djurado, L. Perez, N.W. De Reca, Metastable forms of the tetragonal phase in compositionally homogeneous, nanocrystalline zirconia–ceria powders synthesised by gel-combustion, J. Mater. Chem. 13 (2003) 904–910.
[26] G. Witz, V. Shklover, W. Steurer, S. Bachegowda, H.P. Bossmann, Phase evolution in yttria-stabilized zirconia thermal barrier coatings studied by Rietveld refinement of X-ray powder diffraction patterns, J. Am. Ceram. Soc. 90 (9) (2007) 2935–2940.
[27] B. Henderson, W.D. Emmerich, E. Wassmer, specific heat and energetics of curing and decomposition of a glass-filled polymer composites, Netzsch-Gerätebau GmbH, Selb, Germany (1988).
[28] S. Ahmaniemi, M. Vippola, P. Vuoristo, T. Mantyla, F. Cernuschi, L. Lutterotti, Modified thick thermal barrier coatings: microstructural characterization, J. Eur. Ceram. Soc. 24 (2004) 2247–2258.
[29] G.M. Ingo, T. De Caro, Chemical aspects of plasma spraying of zirconia-based thermal barrier coatings, Acta Mater. 56 (2008) 5177–5187.
[30] D. Chen, M. Gell, E.H. Jordan, E. Cao, X. Ma, Thermal stability of air plasma spray and solution precursor plasma spray thermal barrier coatings, J. Am. Ceram. Soc. 90 (10) (2007) 3160–3166.
[31] N. Wang, C. Zhou, S. Gong, H. Xu, Heat treatment of nanostructured thermal barrier coating, Ceram. Int. 33 (2007) 1075–1081.
[32] S. Sodeoka, M. Suzuki, K. Ueno, H. Sakuramoto, T. Shibata, M. Ando, Thermal and mechanical properties of ZrO_2–CeO_2 plasma-sprayed coatings, J. Thermal Spray Technol. 6 (3) (1997) 361–367.
[33] S. Ahmaniemi, P. Vuoristo, T. Mantyla, F. Cernuschi, L. Lorenzoni, Modified thick thermal barrier coatings: thermophysical characterization, J. Eur. Ceram. Soc. 24 (2004) 2669–2679.
[34] R. Vassen, X. Cao, F. Tietz, D. Basu, D. Stover, Zirconates as new materials for thermal barrier coatings, J. Am. Ceram. Soc. 83 (8) (2000) 2023–2028.
[35] W. Chi, S. Sampath, H. Wang, Microstructure-thermal conductivity relationship for plasma-sprayed yttria-stabilized zirconia coatings, J. Am. Ceram. Soc. 91 (8) (2008) 2636–2645.